PHYSICAL REVIEW C **87**, 051301(R) (2013)

Use of the discrete variable representation basis in nuclear physics

Aurel Bulgac[1] and Michael McNeil Forbes[1,2]
[1]*Department of Physics, University of Washington, Seattle, Washington 98195, USA*
[2]*Institute for Nuclear Theory, University of Washington, Seattle, Washington 98195, USA*
(Received 31 January 2013; revised manuscript received 26 March 2013; published 3 May 2013)

The discrete variable representation (DVR) basis is nearly optimal for numerically representing wave functions in nuclear physics: Suitable problems enjoy exponential convergence, yet the Hamiltonian remains sparse. We show that one can often use smaller basis sets than with the traditional harmonic oscillator basis, and still benefit from the simple analytic properties of the DVR bases which require no overlap integrals, simply permit using various Jacobi coordinates, and admit straightforward analyses of the ultraviolet and infrared convergence properties.

DOI: 10.1103/PhysRevC.87.051301 PACS number(s): 21.60.−n, 21.10.−k, 03.65.Ge

Problems in nuclear physics typically require solving the one-body Schrödinger equation in three dimensions. Numerically representing wave functions requires limiting both ultraviolet (UV) and infrared (IR) scales: a finite spatial resolution (i.e., a lattice) characterizes the highest representable momenta Λ, while a finite size (i.e., a cubic box of volume L^3) determines the largest physical extent. Nuclear structure calculations are historically dominated by the use of the harmonic oscillator (HO) basis of HO wave functions. The appeal of the HO basis stems from the shape of the self-consistent field obtained for small nuclei, which can be approximated by a harmonic potential at small distances from the center of the nucleus. One can also use the Talmi-Moshinsky transformation to separate out the center-of-mass motion in products of single-particle HO wave functions. Recent efforts have been made to determine a minimal HO basis set, and to understand its convergence and accuracy [1,2].

Here we advocate that the discrete variable representation (DVR)—in particular the Fourier plane-wave basis—enjoys most of the advantages of the HO basis, but with a significant improvement in terms of computational efficiency and simplicity, thereby admitting straightforward UV and IR convergence analyses and implementation.

Consider wave functions in a cubic box of volume L^3 with momenta less than Λ. The total number of quantum states in such a representation is given by the following intuitive formula—the ratio of the total phase space volume to the phase space volume of a single three-dimensional (3D) quantum state:

$$\mathcal{N}_{\text{QS}} = \left(\frac{L\ 2\Lambda}{2\pi\hbar}\right)^3. \tag{1}$$

One obtains the same result [3] using Fourier analysis: there are exactly $\mathcal{N}_{\text{QS}}$ linearly independent functions in a cubic 3D box of volume L^3 with periodic boundary conditions and wave vectors less than $k_c = \Lambda/\hbar$ in each direction. These can be conveniently represented in the coordinate representation with N equally spaced points in each direction and lattice constant $a = \pi/k_c = \pi\hbar/\Lambda = L/N$ for a total of $N^3 = \mathcal{N}_{\text{QS}}$ coefficients. The maximum wave vector k_c is simply the Nyquist frequency [3]; one gains nothing by sampling the functions on intervals ("times") finer than a.

The wave functions can also be represented in momentum space using a discrete fast Fourier transform (FFT) [4]. The momentum representation consists of $\mathcal{N}_{\text{QS}}$ coefficients on a 3D cubic lattice with spacing $2\pi\hbar/L$ and extent $-\Lambda \leqslant p_{x,y,z} < \Lambda$. Using the FFT to calculate spatial derivatives is not only fast with $N \log N$ scaling, but extremely accurate—often faster and more accurate than finite-difference formulas. We use an even number of lattice points ($N = 2^n$ is best for the FFT) and quantize the three momenta ($p_{x,y,z} = \hbar k_{x,y,z}$)

$$p_k = \frac{2\pi k\hbar}{L}, \quad x_k = ak,$$
$$k \in \left(-\tfrac{N}{2}, -\tfrac{N}{2}+1, \ldots, \tfrac{N}{2}-1\right). \tag{2}$$

The Fourier basis uses plane waves—e.g. $\exp(ik_n x)$ in the x direction—but these can be linearly combined to form an equivalent sinc-function basis:

$$\psi_k(x) = \operatorname{sinc} k_c(x - x_k) = \frac{\sin k_c(x - x_k)}{k_c(x - x_k)}. \tag{3}$$

This is similar to the difference between Bloch and Wannier wave functions in condensed matter physics. An advantage of this basis is that it is quasi-local $\psi_k(x_l) = \delta_{kl}$ allowing one to represent external potentials as a diagonal matrix $V_{kl} \approx V(x_k)\delta_{kl}$ [see Eq. (19)].

The plane-wave basis can thus be interpreted as a periodic DVR basis set, which has been discussed extensively in the literature (see [5–9] and the references therein), and one can take advantage of Fourier techniques and the useful DVR properties.

In general, DVR bases are characterized by two scales: a UV scale $\Lambda = \hbar k_c$ defining the largest momentum representable in the basis, and an IR scale L defining the maximum extent of the system. In many cases, the basis is constructed by projecting Dirac δ functions onto the finite-momentum subspace. For example, the sinc-function basis (3) is precisely the set of projected Dirac δ functions $\psi_n(x) = P_{p\leqslant\Lambda}\delta(\boldsymbol{r} - \boldsymbol{r}_\alpha)$ onto the subspace $|\boldsymbol{p}| \leqslant \Lambda$ [5–7]. (It can be nontrivial, however, to choose a consistent set of abscissa maintaining the quasi-locality property.) The basis thus optimally covers the region $[-L/2, L/2) \times [-\Lambda, \Lambda)$ for each axis in phase space, and leads to an efficient discretization scheme with exponential convergence properties.

The DVR basis admits a straightforward analysis of the UV and IR limits, allowing one to construct effective extrapolations to the continuum and thermodynamic limits, respectively. The UV effects may be analyzed by simply considering the properties of the projection $P_{p\leqslant\Lambda}$ used to define the basis, and the IR limit for the periodic basis is well understood by techniques like those derived by Beth, Uhlenbeck, and Lüscher [10,11]. We would like to emphasize an additional technique here: The IR limit is characterized by $2\pi\hbar/L$—the smallest interval in momentum space resolvable with the basis set. For some problems, one can efficiently circumvent this limitation by using "twisted" boundary conditions $\psi(\boldsymbol{r}+\boldsymbol{L}) = \exp(\mathrm{i}\theta_B)\psi(\boldsymbol{r})$ or Bloch waves as they are known in condensed matter physics. In particular, averaging over $\theta_B \in [0, 2\pi)$ will completely remove any IR limitations (without changing the basis size) for periodic and homogeneous problems, effectively "filling-in" the momentum states $p_n \leqslant p_n + \hbar\theta_B/L < p_{n+1}$. Extensions of these formulas to the case of a box with unequal sides is straightforward.

To demonstrate the properties of the DVR basis, we contrast it with the HO basis. The periodic DVR basis (plane waves) shares the ease of separating out the center of mass. In particular, one can use Jacobi coordinates to separate out the center-of-mass motion without evaluating Talmi-Moshinsky coefficients, leading to simpler and more transparent implementations. The quasi-locality of the DVR basis offers an additional implementation advantage over the HO basis: one need not compute wave-function overlaps to form the potential energy matrix. In contrast with the HO basis, the kinetic energy matrix $\boldsymbol{K}$ is no longer diagonal, but it has an explicit formula (23), and is quite sparse, unlike the potential energy operator in the HO basis.

Consider the HO wave functions with energy $E \leqslant \hbar\omega(N + 3/2)$: the maximum radius and momenta are

$$R = \sqrt{2N+3}\,b, \quad \Lambda = \sqrt{2N+3}\,\frac{\hbar}{b}, \tag{4}$$

where $b = \sqrt{\hbar/m\omega}$ is the oscillator length. For large N, $N \approx R\Lambda/2\hbar$. Thus, to expand a wave function with extent $2R$ containing momenta $|p| < \Lambda$ requires at least

$$\mathcal{N}_{\mathrm{HO}} = \frac{(N+1)(N+2)(N+3)}{6} \approx \frac{1}{6}\left(\frac{R\Lambda}{2\hbar}\right)^3 \tag{5}$$

states. To contrast, the DVR basis covering the required volume of phase space (1) with $L = 2R$ and Λ is

$$\mathcal{N}_{\mathrm{DVR}} = \left(\frac{2R\ 2\Lambda}{2\pi\hbar}\right)^3. \tag{6}$$

The ratio in the limit $N \to \infty$ is thus

$$\frac{\mathcal{N}_{\mathrm{DVR}}}{\mathcal{N}_{HO}} = \frac{384}{\pi^3} \approx 12.4. \tag{7}$$

Since these states are localized, one can further impose Dirichlet boundary conditions, allowing functions only of the type $\sin(k_n x)$ with $k_n L = n\pi$ [instead of $\exp(ik_n x)$], thereby keeping only half of the momenta:

$$\frac{\mathcal{N}_{\mathrm{DVR}}}{\mathcal{N}_{\mathrm{HO}}} = \frac{48}{\pi^3} \approx 1.5. \tag{8}$$

Choosing a cubic box with Dirichlet boundary conditions, sides $L = 40$ fm, and maximum momentum $\Lambda = 300\,\mathrm{MeV/c}$ gives

$$\mathcal{N}_{\mathrm{DVR}} = \left(\frac{L\ \Lambda}{2\pi\hbar}\right)^3 \approx 10^3, \tag{9}$$

a somewhat surprisingly small number of states. For symmetric states, one could further reduce the basis by imposing cubic symmetry, decreasing the basis size by another factor of 8.

Finally, one can fully utilize spherical symmetry with a related Bessel-function DVR basis gaining a factor of $\pi/6$, and thereby besting the HO basis

$$\frac{\mathcal{N}_{\mathrm{DVR}}}{\mathcal{N}_{\mathrm{HO}}} = \frac{8}{\pi^2} \approx 0.8 < 1. \tag{10}$$

In this counting, spin and isospin degrees of freedom which occur in both bases have been omitted.

The Bessel-function DVR basis set [5–7,12] follows from a similar procedure of projecting Dirac δ functions for the radial Schrödinger equation. The angular coordinates are treated in the usual manner using spherical harmonics, but the radial wave functions are based on the Bessel functions (see Refs. [7,12] for details) which satisfy the orthogonality conditions

$$\int_0^{k_c} dk\,\frac{2k}{k_c^2}\,\frac{J_\nu(kr_{\nu\alpha})J_\beta(kr_{\nu\beta})}{|J'_\nu(kr_{\nu\alpha})J'_{\nu\beta}(kr_{\nu\beta})|} = \delta_{\alpha\beta}, \tag{11}$$

where $z_{\nu\alpha} = k_c r_{\nu\alpha}$ [the zeros of the Bessel functions $J_\nu(z_{\nu\alpha}) = 0$] define the radial abscissa $r_{\nu,\alpha}$. The DVR basis set is

$$F_{\nu n}(r) = \sqrt{r}\,J_\nu\left(\frac{z_{\nu n} r}{R}\right), \quad z_{\nu n} = k_c r_{\nu n}. \tag{12}$$

Differential operators have simple forms in the DVR basis (see Refs. [5–7] and the codes [13,14]). In principle, a different basis (and corresponding abscissa) should be used for each angular momentum quantum number ν. In practice, good numerical accuracy is obtained using the $\nu = 0$ basis $j_0(z_{0n}r/R)$ and the $\nu = 1$ basis $j_1(z_{1n}r/R)$, respectively, for even and odd partial waves [12,13]. In the S-wave case, the abscissa are simply the zeros of the spherical Bessel function $j_0(z) = \sin(z)/z$:

$$z_{0n} = n\pi, \quad r_{0n} = \frac{n\pi}{k_c}, \quad n = 1, 2, 3, \ldots, N, \tag{13}$$

and correspond to the 1D basis with Dirichlet boundary conditions mentioned earlier. The zeros for $j_1(z)$ lie between the zeros of $j_0(z)$. The number of DVR functions needed to represent with exponential accuracy a radial wave function is

$$\mathcal{N}_{0\,\mathrm{DVR}} = \frac{Rk_c}{\pi}, \tag{14}$$

to be compared (in the limit $N \to \infty$) with

$$\mathcal{N}_{0\,\mathrm{HO}} = \frac{Rk_c}{4}. \tag{15}$$

In the last formula we have divided by an additional factor of 2, since $N = 2n + l$ changes in steps of 2.

A major drawback of the HO wave functions that is rarely mentioned is that, for modest values of N and $l \neq 0$, the radial wave functions concentrate in two distinct regions: around

the inner and outer turning points of the effective potential $V(r) = \hbar^2 l(l+1)/2mr^2 + m\omega^2 r^2/2$. By adding components with larger values of N, one modifies the wave function at both small and large distances, leading to slow convergence. In contrast, the DVR functions are concentrated around a single lattice site. Thus, adding more components only affects the solution in the vicinity of the additional lattice points, leaving the states largely unaffected elsewhere.

For nuclei one can gain insight with some estimates. Cutoffs of $\Lambda = 600\,\mathrm{MeV/c}$ and $R = 1.5 \cdots 2A^{1/3}$ fm should satisfy most of the practical requirements, leading to

$$b = \sqrt{\frac{\hbar R}{\Lambda}} \approx 0.7 \cdots 0.8 A^{1/6}\ \mathrm{fm}, \tag{16a}$$

$$\hbar\omega = \frac{\hbar^2}{mb^2} = \frac{\hbar\Lambda}{mR} \approx 60 \cdots 80 A^{-1/3}\ \mathrm{MeV}, \tag{16b}$$

compared to the value $40A^{-1/3}$ MeV one finds in typical monographs [15]. Using only half the value of $\Lambda = 300\,\mathrm{MeV/c}$ naturally halves the value of $\hbar\omega$.

We end with demonstrations of the DVR method [14]. We start with the harmonic oscillator problem in 1D

$$H\phi(x) = \left(-\frac{\hbar^2}{2m}\frac{d^2}{dx^2} + \frac{k_c^2 x^2}{2R^2}\right)\phi(x) = E\phi(x), \tag{17}$$

where we choose the harmonic oscillator frequency according to Eq. (16b), varying the lattice constant $a = \pi/k_c$ and $L = Na$. The DVR method is sometimes referred to as the Lagrange method in numerical analysis [9], and functions are usually represented on the spatial lattice

$$\psi(x) = \sum_k a\psi(x_k) f_k(x), \quad \langle f_k | f_l \rangle = \delta_{kl}. \tag{18}$$

Potential matrix elements usually have a simple and unexpectedly accurate representation (quasi-locality)

$$\langle f_k | V | f_l \rangle = \int dx f_k^*(x) V(x) f_l(x) \approx V(x_k)\delta_{kl}, \tag{19}$$

where the functions $f_k(x)$ are a linear combination of plane waves and form an orthonormal set (these formulas apply for even numbers of abscissa as required by efficient implementations of the FFT)

$$f_k(x_l) = \sum_{n=-N/2}^{N/2-1} \frac{1}{L} \exp\frac{ip_n(x_l - x_k)}{\hbar} = \begin{cases} \frac{\sin\pi(k-l)}{Na} \cot\frac{\pi(k-l)}{N} = 0 & k \neq l, \\ 1/a & k = l, \end{cases} \tag{20}$$

$$\psi(x_k) = \sum_l a f_k(x_l)\psi(x_l), \tag{21}$$

where x_k and p_n were defined in Eq. (2). As before, the functions $f_k(x_l)$ are simply the normalized projections of the periodic Dirac functions on the DVR subspace [5–7], and satisfy

$$\sum_n a f_k(x_n) f_l(x_n) = \delta_{kl}. \tag{22}$$

The sinc-function basis (3) is obtained in the limit $N \to \infty$ (if $a = 1$). Similar formulas exist for the calculation of various other spatial derivatives.

While the potential matrix is diagonal, the DVR kinetic energy is a matrix in coordinate representation:

$$K_{kl} = \begin{cases} \frac{\hbar^2\pi^2}{mN^2a^2} \frac{(-1)^{k-l}}{\sin^2\frac{\pi(k-l)}{N}} & k \neq l \\ \frac{\hbar^2\pi^2}{6ma^2}\left(1 + \frac{2}{N^2}\right) & k = l. \end{cases} \tag{23}$$

This matrix is full matrix in 1D, but sparse in 3D where only $1/N^2$ of the matrix elements are nonvanishing. The HO Hamiltonian (17) is thus represented in the DVR basis with periodic boundary conditions as

$$H_{kl} = K_{kl} + \frac{m\omega^2 a^2 k^2}{2}\delta_{kl}. \tag{24}$$

The implementation of Dirichlet boundary conditions uses the $\nu = 0$ Bessel function basis (see the MATLAB code [13] for $l = 0$ and also Ref. [9] for other possible DVR basis sets in 1D).

In Fig. 1 we show the energy differences between the eigenvalues of the Hamiltonian (24) and $\hbar\omega(n + 1/2)$. These "errors" are indicative only of the energy shifts due to the tunneling between neighboring cells in the case of periodic boundary conditions, as one can judge by comparing systems with different lengths at the same energy, when the tunneling matrix elements are similar. The results for the lowest 2/3 of the spectrum are, for all practical purposes, converged in the DVR method, and the harmonic oscillator basis set is worse in this case. With $N = Lk_c/4 \approx 24$ one can obtain at most 10 states or so with a reasonable accuracy in this

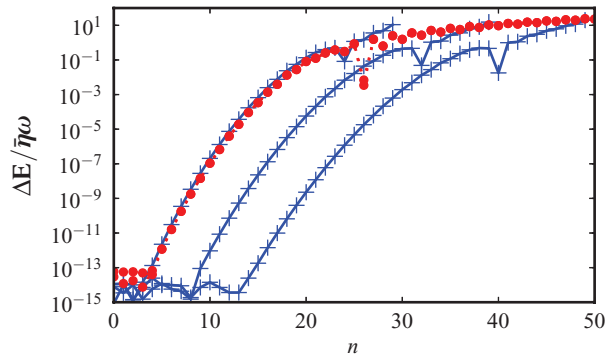

FIG. 1. (Color online) Difference in spectrum between the DVR Hamiltonian (24) and the HO energies $(n + 1/2)\hbar\omega$. The three (blue) curves with pluses have fixed UV scale (lattice constant $a = 1$, $k_c = \pi/a$) with $L = \in \{30, 40, 50\}$ and $\omega = 2\pi/L$ from left to right. The (red) curves with dots have fixed $L = 30$ but varying lattice constant $a \in \{1/2, 1/3\}$ demonstrating the UV convergence. The sizes of the DVR basis sets are $Lk_c/\pi = 30$, 40, and 50 (blue pluses) and 60 and 90 (red circles), respectively. For the blue pluses, the corresponding number of HO wave functions suggested in Refs. [1,2] [see also Eqs. (4)] would be $N = Lk_c/4 = L\pi/4a \approx 24$, 31, 39; and 47 and 71 for the red dots, respectively. Notice that the size of the DVR basis set can be reduced by a factor of 2 to $Lk_c/2\pi = 15$, 20, 25 (blue) and 30, 45 (red) respectively, by imposing Dirichlet boundary conditions; however, in that case, states not localized to a single cell will not be reproduced.

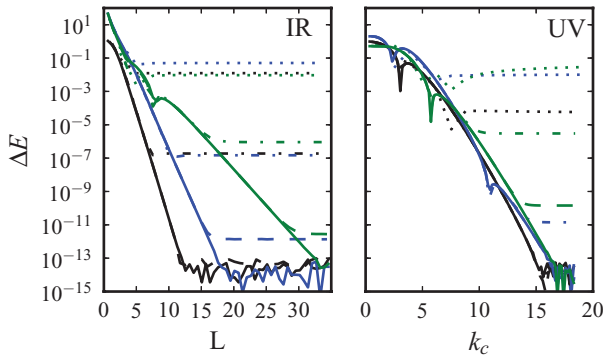

FIG. 2. (Color online) Exponential convergence of the periodic DVR basis for the energy of the bound states of the analytically solvable Scarf II potential $V(x) = [a + b\sinh x]/\cosh^2 x$ (with $\hbar = m = 1$). For $a = 7/2$ and $b = -11/2$, the potential has three bound states: $E_n = -(3-n)^2/2$ (shown in black, blue, and green from left to right, respectively). The left plot demonstrates the IR convergence for increasing L with fixed k_c; the right plot, the UV convergence for increasing k_c for fixed L. The various values for $k_c \in \{5, 10, 15, 20\}$ (left) and $L \in \{5, 15, 25, 35\}$ (right) correspond to dotted, dot-dashed, dashed, and solid lines with increasing convergence, respectively.

reduced interval on the x axis with periodic or Dirichlet boundary conditions, if one were to follow the prescription of Refs. [1,2].

In Fig. 2 we demonstrate the UV and IR exponential convergence of the DVR method for an asymmetric short-range potential with analytic wave functions. Note that both IR and UV errors scale exponentially until machine precision is achieved: $\Delta E \propto \exp[-2k(L)L]$ (IR) and $\Delta E \propto \exp(-2k_c r_0)$ (UV), respectively, where r_0 is potential dependent and $k(L)$ is determined by the bound state energy $E(L) = -\hbar^2 k^2(L)/2m$. These exponential scalings follow from simple Fourier analysis (UV) and band structure theory (IR) for short-range smooth potentials. Note in particular that the linear UV scaling differs from the quadratic empirical dependence discussed in [1]. We have also demonstrated the utility of the DVR method for a variety of density functional theory (DFT) and quantum Monte Carlo (QMC) many-body calculations.

The Bessel-function DVR basis $j_l(\Lambda r_n/\hbar)$ for spherical coordinates was used in [13,16] to solve the self-consistent superfluid local density approximation (SLDA) DFT equations for the harmonically trapped unitary Fermi gas. While the basis is defined for all l, even and odd l-partial radial wave functions can be effectively expressed using only the j_0 and j_1 basis sets, respectively (see [12]), with the angular coordinates represented by spherical harmonics. The spatial mesh size is given by $\Delta r = r_{n+1} - r_n \approx \pi\hbar/\Lambda$. Applied to nuclear matter, $\Lambda = 600$ MeV/c gives $\Delta r \approx 1$ fm and $N_s = R/\Delta r \approx 20$ radial mesh points in a spherical box of radius $R \approx 20$ fm. A MATLAB code for a spin imbalanced trapped unitary gas with pairing and using two different chemical potentials for the spin-up and spin-down fermions is about 400 lines and converges in a few seconds on a laptop [13,14].

The periodic DVR basis was used in Ref. [17] to solve the self-consistent SLDA DFT, predicting a supersolid Larkin-Ovchinnikov (LO) phase in the spin imbalanced unitary Fermi gas. Explicit summation over Bloch momenta was used to remove any IR errors (i.e., simulating a periodic state in infinite space rather than in a periodic space). The periodic basis was also used in [18] to demonstrate the Higgs mode by solving the time-dependent SLDA for systems with up to 10^5 particles. (In both these approaches, spatial variations were only allowed in one direction: transverse directions were treated analytically.)

Full 3D periodic DVR bases were used in [19] to solve the time-dependent SLDA equations for $48 \times 48 \times 48$ and $196 \times 32 \times 32$ lattices, solving $\approx 5 \times 10^5$ nonlinearly coupled partial-differential equations for several million time steps to study the real-time dynamics of the superfluid unitary Fermi gas. Extensions of this code on current supercomputers allow us to increase the overall size of such problems by an order of magnitude. These 3D DVR bases were also used to study the giant dipole resonance (GDR) in deformed triaxial open-shell heavy nuclei [20] without any symmetry restrictions. Finally, the 3D DVR basis was used in [21] (and earlier references therein) to perform *ab initio* QMC calculations of strongly interacting fermions in spatial lattices ranging from $6^3 = 216$ to $16^3 = 4096$ for systems comprising 20–160 particles and with 5000 steps in imaginary time. These systems are significantly larger than the 364 single-particle states used in [22] to implement a nuclear shell-model QMC [23]. Similar applications of DVR QMC are currently being developed for nuclear systems.

We further illustrate the power of the DVR basis in Fig. 3 by solving the 6D and 9D Schrödinger equations for three-body ("triton") and four-body ("α") bound states with distinguishable particles interacting with two centrally symmetric potentials: a purely attractive Posh-Teller potential, and an attractive potential with a repulsive core (see the inset). We used a Cartesian lattice for the relative Jacobi coordinates to eliminate the center-of-mass coordinate. Our goal was to solve these with a modern laptop (2.7 GHz Intel Core i7 MacBook Pro with 16 GB of RAM) in no more than about a few minutes, without any tricky optimizations such as taking advantage of symmetry properties of the wave function. (Parity alone could reduce the Hilbert space by factors of 2^6 and 2^9 respectively.) Coding these problems is simple—the MATLAB versions are about 200 lines per problem while the general Python code is about 1000 lines (including documentation and tests) [14]. We are not aware of other attempts to solve directly the Schrödinger equation in a 9D space.

To compute the ground-state energy, we use two alternative techniques: imaginary time evolution of a trial state (slow convergence but gives a representative wave function) and a simple Lanczos algorithm (fast convergence, but only a few low-energy eigenvalues). For the triton we used lattices $N_s^6 = 8^6 \cdots 16^6$: for the α state we use lattices $N_s^9 = 4^9 \cdots 8^9$. The size of the largest Hilbert space is thus $\approx 1.68 \times 10^7$ for the triton and $8^9 \approx 1.34 \times 10^8$ for the α. Several spatial mesh sizes $a = 0.5$–1.5 fm corresponding to $\Lambda \approx 300$–930 MeV/c are used to explore convergence. Note that, unlike with other methods used for nuclear structure calculations, adding local three-body and four-body interactions will neither complicate the code nor impact the performance.

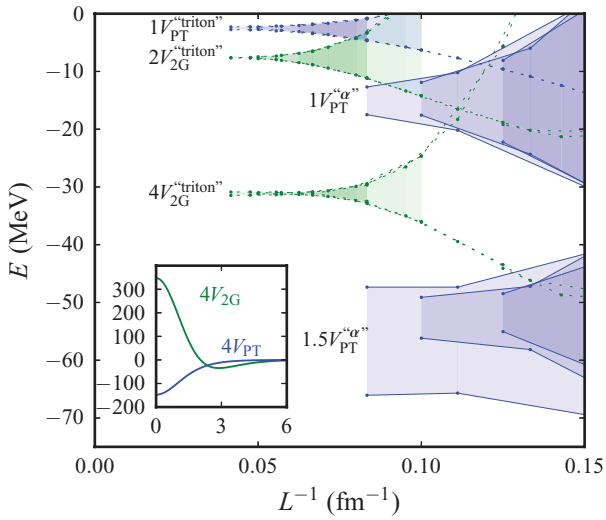

FIG. 3. (Color online) Binding energy of a three-particle "triton" and four-particle "α" ground state using various multiples (specified by numerical factors in the figure) of the potentials $V_{\rm PT}(r) \propto -{\rm sech}^2(2r/r_0)$ and $V_{\rm 2G}(r) \propto \exp(-r^2/r_0^2) - 4\exp(-4r^2/r_0^2)$ with $r_0 = 3$ fm (see [24] for explicit normalizations). Upper and lower bounds are obtained from Dirichlet and periodic boundary conditions, respectively. The deeply bound four-body state with $1.5V_{\rm PT}$ is not converged and has comparable UV and IR errors (each "band" has fixed lattice spacing). The other results are UV converged: the different lattice spacings lying on the same curves describing the dependence on the box size. The inset shows the radial profile of the two potentials.

As discussed earlier, the UV convergence is determined by the properties of the interaction. For example, the high-momentum components of a wave function in a short-range potential will have a power-law decay $\propto k^{-4}$ [25] (rather than an exponential decay). The IR convergence of the energy will be determined by the energy of the lowest many-body threshold. For example, if there is an S-wave two-body threshold with binding energy difference $Q(L)$ in the box, then the IR error will be [11]

$$E(L) \approx E_\infty + \frac{A\exp[-\sqrt{2MQ(L)}L/\hbar]}{L}, \qquad (25)$$

where M is the corresponding reduced mass, and A an asymptotic normalization factor that is positive or negative for Dirichlet or periodic boundary conditions respectively. If the lowest threshold is higher-body or in a different (not S-wave) configuration, then this behavior will be modified in a straightforward manner. (Competition between several closely lying thresholds will further complicate the IR convergence properties.) Note that this differs from the results of [1].

In summary, the DVR basis seems ideal for nuclear structure calculations using either DFT, QMC, or configuration mixing approaches. It is near optimal in size and can deliver results with exponential convergence. The DVR basis shares the important advantages of the HO basis set: efficiently separating out the center-of-mass motion using Jacobi coordinates (with the added benefit of not needing to evaluate Talmi-Moshinsky coefficients), utilizing symmetries to reduce the basis size (spherical with the Bessel function DVR). Moreover, matrix elements are easy to evaluate: the potential matrix is diagonal for local potentials [no overlap integrals are needed; see, for example, Eq. (19)], the kinetic energy matrix is sparse and explicitly expressed analytically, and many-body forces can be easily included. Furthermore, the UV and IR convergence properties of the basis appear on a equal footing and are clearly expressed in terms of the momentum-space projection and finite box size, allowing a simplified and sound convergence analysis, with a clear mathematical underpinning. Finally, we demonstrated that the DVR basis can be used in extremely large Hilbert spaces with relatively modest computational resources.

We thank G. F. Bertsch for discussions and the support under US DoE Grants No. DE-FG02-97ER41014, No. DE-FC02-07ER41457, and No. DE-FG02-00ER41132.

[1] R. J. Furnstahl, G. Hagen, and T. Papenbrock, Phys. Rev. C **86**, 031301(R) (2012).
[2] S. A. Coon, M. I. Avetian, M. K. G. Kruse, U. van Kolck, P. Maris, and J. P. Vary, Phys. Rev. C **86**, 054002 (2012).
[3] R. W. Hamming, *Numerical Methods for Scientists and Engineers* (McGraw-Hill, New York, 1973).
[4] "The Fastest Fourier Transform in the West," www.fftw.org, developed by M. Frigo and S. G. Johnson.
[5] R. G. Littlejohn and M. Cargo, J. Chem. Phys. **116**, 7350 (2002).
[6] R. G. Littlejohn, M. Cargo, T. Carrington, Jr., K. A. Mitchell, and B. Poirier, J. Chem. Phys. **116**, 8691 (2002).
[7] R. G. Littlejohn and M. Cargo, J. Chem. Phys. **117**, 27 (2002).
[8] D. Baye, J. Phys. B **28**, 4399 (1995).
[9] D. Baye, Phys. Status Solidi B **243**, 1095 (2006).
[10] E. Beth and G. E. Uhlenbeck, Physica **4**, 915 (1937).
[11] M. Lüscher, Comm. Math. Phys. **104**, 177 (1986); S. R. Beane, P. F. Bedaque, A. Parreño, and M. J. Savage, Phys. Lett. B **585**, 106 (2004).
[12] N. Nygaard, G. M. Bruun, B. I. Schneider, C. W. Clark, and D. L. Feder, Phys. Rev. A **69**, 053622 (2004).
[13] http://www.phys.washington.edu/~bulgac/numerical_programs.html
[14] https://bitbucket.org/mforbes/paper_dvrvsho
[15] A. Bohr and B. R. Mottelson, *Nuclear Structure* (World Scientific, Singapore, 1998).
[16] A. Bulgac, Phys. Rev. A **76**, 040502 (2007).
[17] A. Bulgac and Michael McNeil Forbes, Phys. Rev. Lett. **101**, 215301 (2008).
[18] A. Bulgac and S. Yoon, Phys. Rev. Lett. **102**, 085302 (2009).

[19] A. Bulgac, Y.-L. Luo, and K. J. Roche, Phys. Rev. Lett. **108**, 150401 (2012).
[20] I. Stetcu, A. Bulgac, P. Magierski, and K. J. Roche, Phys. Rev. C **84**, 051309(R) (2011).
[21] G. Wlazlowski, P. Magierski, J. E. Drut, A. Bulgac, and K. J. Roche, Phys. Rev. Lett. **110**, 090401 (2013); J. E. Drut, T. A. Lähde, G. Wlazłowski, and P. Magierski, Phys. Rev. A **85**, 051601 (2012).
[22] C. N. Gilbreth and Y. Alhassid, arXiv:1210.4131.
[23] S. E. Koonin, D. J. Dean, and K. Langanke, Phys. Rep. **278**, 1 (1997).
[24] Michael McNeil Forbes, S. Gandolfi, and A. Gezerlis, Phys. Rev. A **86**, 053603 (2012).
[25] R. Sartor and C. Mahaux, Phys. Rev. C **21**, 1546 (1980); S. Tan, Ann. Phys. (NY) **323**, 2971 (2008).